



## RESEARCH ARTICLE

10.1029/2022JG007291

### Key Points:

- Small rivers are major contributors of CO<sub>2</sub> emissions despite their low CO<sub>2</sub> concentrations and small surface areas
- Anthropogenic land use changes can enhance land–river carbon transport and riverine CO<sub>2</sub> emissions
- Strong CO<sub>2</sub> emissions during the wet season suggest that seasonal variation must be considered when evaluating riverine CO<sub>2</sub> emissions

### Supporting Information:

Supporting Information may be found in the online version of this article.

### Correspondence to:

L. Ran,  
lsran@hku.hk

### Citation:



Liu, B., Wang, Z., Tian, M., Yang, X., Chan, C. N., Chen, S., et al. (2023). Basin-scale CO<sub>2</sub> emissions from the East River in South China: Importance of small rivers, human impacts and monsoons. *Journal of Geophysical Research: Biogeosciences*, 128, e2022JG007291. <https://doi.org/10.1029/2022JG007291>

Received 17 NOV 2022  
Accepted 2 JAN 2023

### Author Contributions:

**Conceptualization:** Boyi Liu, Lishan Ran  
**Data curation:** Boyi Liu, Zifeng Wang  
**Formal analysis:** Boyi Liu, Zifeng Wang  
**Funding acquisition:** Lishan Ran  
**Investigation:** Boyi Liu, Mingyang Tian, Chun Ngai Chan, Shuai Chen, Qianqian Yang  
**Methodology:** Boyi Liu, Zifeng Wang  
**Software:** Zifeng Wang  
**Supervision:** Lishan Ran  
**Writing – original draft:** Boyi Liu  
**Writing – review & editing:** Chun Ngai Chan, Lishan Ran

# Basin-Scale CO<sub>2</sub> Emissions From the East River in South China: Importance of Small Rivers, Human Impacts and Monsoons

Boyi Liu<sup>1</sup> , Zifeng Wang<sup>1</sup>, Mingyang Tian<sup>2</sup>, Xiankun Yang<sup>3</sup>, Chun Ngai Chan<sup>4</sup>, Shuai Chen<sup>1</sup>, Qianqian Yang<sup>1</sup>, and Lishan Ran<sup>1</sup> 

<sup>1</sup>Department of Geography, The University of Hong Kong, Pokfulam, Hong Kong, <sup>2</sup>Center for Earth System Research and Sustainability (CEN), Institute for Geology, Universität Hamburg, Hamburg, Germany, <sup>3</sup>School of Geographical Sciences, Guangzhou University, Guangzhou, China, <sup>4</sup>Department of Biological Sciences, University of Lethbridge, Lethbridge, AB, Canada

**Abstract** Riverine carbon dioxide (CO<sub>2</sub>) emissions are an essential component of the riverine carbon cycle, but an accurate assessment of riverine CO<sub>2</sub> emission fluxes is still hindered by the spatial and temporal variations among river basins caused by differences in climate, watershed characteristics, and human activity. Here, we evaluate the riverine CO<sub>2</sub> flux from the subtropical East River Basin (ERB) in south China, a region strongly affected by monsoon climate and anthropogenic land use changes. Our results suggest small rivers are major contributors to riverine CO<sub>2</sub> emissions, even with relatively low CO<sub>2</sub> concentrations and small water surface areas (SAs). They contribute disproportionately to 74.4% of the total fluxes due to high gas transfer velocity ( $k$ ) across the water–air interface. Land use changes have substantially enhanced CO<sub>2</sub> emissions from river networks. Normalized areal riverine CO<sub>2</sub> fluxes in the urban- and cropland-dominated Middle and Lower ERB (27.6 and 39.4 g C m<sup>-2</sup> yr<sup>-1</sup>) were two and three times higher than the 9.1 g C m<sup>-2</sup> yr<sup>-1</sup> in the forest-dominated Upper ERB. Due to the larger water SA and higher  $k$  caused by monsoon-induced precipitation, the East River acts as a stronger carbon source during the wet season, emitting 0.67 Tg C yr<sup>-1</sup> to the atmosphere, which is about twice that during the dry season (0.33 Tg C yr<sup>-1</sup>). Our study illustrated how monsoon climate and land use in the ERB have regulated its riverine CO<sub>2</sub> emissions. Our findings also provided valuable insights into the role of small rivers in the basin-wide carbon cycle.

**Plain Language Summary** An accurate calculation of carbon dioxide (CO<sub>2</sub>) emitted from rivers to the atmosphere is important for a better understanding of the carbon cycle in river basins. However, the lack of studies in some hotspots of riverine CO<sub>2</sub> emissions has hampered the accuracy of the current estimate. Here, we evaluate the amount of riverine CO<sub>2</sub> emitted from the subtropical East River Basin (ERB) in south China. Our results suggest that small rivers are major sources of CO<sub>2</sub> emissions, responsible for around three-fourths of the total emissions. Meanwhile, human-induced land use changes have substantially enhanced CO<sub>2</sub> emissions from rivers. Areal riverine CO<sub>2</sub> emissions in the urban- and cropland-dominated Middle and Lower ERB were two and three times higher, respectively, than that in the forest-dominated Upper ERB. Furthermore, two-thirds of the annual riverine CO<sub>2</sub> emissions occurred during the wet season from April to September, implying that seasonal variation must be considered when calculating the CO<sub>2</sub> emissions. Our study illustrated how climate and land use in the ERB have regulated its riverine CO<sub>2</sub> emissions. The results shed light on the disproportionate role of small rivers in assessing the carbon cycle from a basin-wide perspective.

## 1. Introduction

River networks are key members in the regional and global carbon (C) cycle (Battin et al., 2009; Cole et al., 2007; Drake et al., 2018). Large quantities of C stabilized by the terrestrial ecosystems are transported from the land to rivers through runoff and groundwater (Regnier et al., 2022), and this land–river C transport could offset terrestrial C gain and diminish the C sequestration capacity of terrestrial ecosystems (Chi et al., 2020; Duvert et al., 2020; Lauerwald et al., 2020). Emission in the form of carbon dioxide (CO<sub>2</sub>) from water to the atmosphere is a primary pathway of those land-derived riverine C. Annual CO<sub>2</sub> emissions from rivers could reach up to 2 Pg C (S. Liu et al., 2022), outpacing the C transported by rivers from the land to the ocean or those buried within the river networks (Regnier et al., 2022). However, there is still great uncertainty in estimations of riverine CO<sub>2</sub>

© 2023. The Authors.

This is an open access article under the terms of the [Creative Commons Attribution License](https://creativecommons.org/licenses/by/4.0/), which permits use, distribution and reproduction in any medium, provided the original work is properly cited.

emissions (Cole et al., 2007; Drake et al., 2018; Raymond et al., 2013; Sawakuchi et al., 2017). An accurate quantification of riverine CO<sub>2</sub> emissions is of great significance for evaluating the land–river C transport, which will help us examine the C sequestration capacity of terrestrial ecosystems and understand basin-scale C balance.

The uncertainty in the assessment of global-scale riverine CO<sub>2</sub> emissions is largely attributable to the spatio-temporal heterogeneity in CO<sub>2</sub> fluxes caused by climate conditions and the unevenly spatial and temporal distribution of accessible data (Lauerwald et al., 2015; Raymond et al., 2013). Climate conditions are a major factor that affects the intensity of riverine CO<sub>2</sub> emissions. Seasonal precipitation and temperature changes control the terrestrial ecosystem production and thus decide the potential of land–river C transport (Duvert et al., 2018). They could also regulate the riverine CO<sub>2</sub> concentration and emissions by altering the hydrological conditions and biogeochemical processes (S. Liu et al., 2022; Schneider et al., 2020). As a result, the amount and intensity of CO<sub>2</sub> emissions from rivers are highly dependent on the climate zone in which they are located (S. Liu et al., 2022; Raymond et al., 2013). However, rivers in some climate zones are substantially underrepresented in current assessments of global riverine CO<sub>2</sub> emissions. Notably, despite widespread recognition of tropical and subtropical river systems as hotspots of CO<sub>2</sub> emissions (Borges et al., 2015; Lauerwald et al., 2020; S. Liu et al., 2022), they remain underrepresented at the global-scale estimations (Lauerwald et al., 2015; Raymond et al., 2013). Particularly, CO<sub>2</sub> emissions from tropical and subtropical rivers in Africa and Asia are still understudied (Borges et al., 2015, 2019; L. Ran et al., 2021). A greater understanding of riverine CO<sub>2</sub> emissions from those currently underrepresented rivers is crucial for a more accurate global-scale estimation.

Underrepresentation of small headwater streams is another important factor causing uncertainty in estimations of riverine CO<sub>2</sub> emissions. The contribution of small rivers to CO<sub>2</sub> emissions has not been well quantified because of a lack of data (Lauerwald et al., 2015; Raymond et al., 2013). However, recent studies suggest that small rivers could be major contributors of CO<sub>2</sub> emissions and disproportionately important in riverine CO<sub>2</sub> emission estimation (Crawford et al., 2015; Mwanake et al., 2022; Schelker et al., 2016). Meanwhile, small rivers also have a strong hydrological connection with their surrounding landscapes (Deirmendjian & Abril, 2018; Duvert et al., 2018), which suggests that CO<sub>2</sub> emissions from those small rivers could vary rapidly due to their response to the changing C input from the terrestrial ecosystem (Clow et al., 2021; Mwanake et al., 2022). Therefore, expanding investigation in small rivers are not only crucial for a better estimation of riverine CO<sub>2</sub> emissions but also for a better understanding of the underlying mechanisms. In addition, intensified human activities in the river basin can modify riverine CO<sub>2</sub> emissions (Borges et al., 2018; Gu et al., 2022). Land use cover changes in the river basin, like urbanization and deforestation, could increase riverine CO<sub>2</sub> emissions by increasing anthropogenic C input and facilitating the transport of soil C from the land to rivers (Drake et al., 2019; Gallay et al., 2018; Regnier et al., 2022; W. Zhang et al., 2021). Dam operation, on the other hand, could interfere with the hydrological condition, which affects the in-stream metabolism (Crawford et al., 2016; Ollivier et al., 2019). Given the increasing human influences worldwide, studies on riverine CO<sub>2</sub> emissions should fully consider the impacts of human activities.

The East River in South China is located in the understudied East Asia. Our recent work (B. Liu et al., 2021) reveal that the spatial and temporal characteristics of riverine CO<sub>2</sub> concentrations in the East River Basin (ERB) are affected by the monsoon climate and human impacts in the region, and various underlying processes in small and large rivers result in their difference in CO<sub>2</sub> emissions. However, it is still unclear how those factors affect the estimate of CO<sub>2</sub> emission fluxes and the regional C budget analysis. Therefore, in this study, we extracted the river network in the ERB based on DEM and high-resolution Sentinel remote sensing images. Combining the field-measured and modeled CO<sub>2</sub> concentration and gas transfer velocity data, CO<sub>2</sub> emission fluxes from the entire East River network were determined. The objectives of this study are to (a) estimate the CO<sub>2</sub> emission fluxes from the river networks in the ERB, (b) evaluate the contribution of small rivers to total riverine CO<sub>2</sub> emissions, (c) examine the impacts of human activities and monsoon climate on riverine CO<sub>2</sub> emissions and their implications for basin-scale riverine CO<sub>2</sub> emission calculation and regional C budget analysis.

## 2. Materials and Methods

### 2.1. Site Description

The East River in the subtropical south China is one of the three major tributaries of the Pearl River system (Figure 1). With an area of 35,400 km<sup>2</sup>, the main stem channel is 562 km long. Due to the monsoon climate,

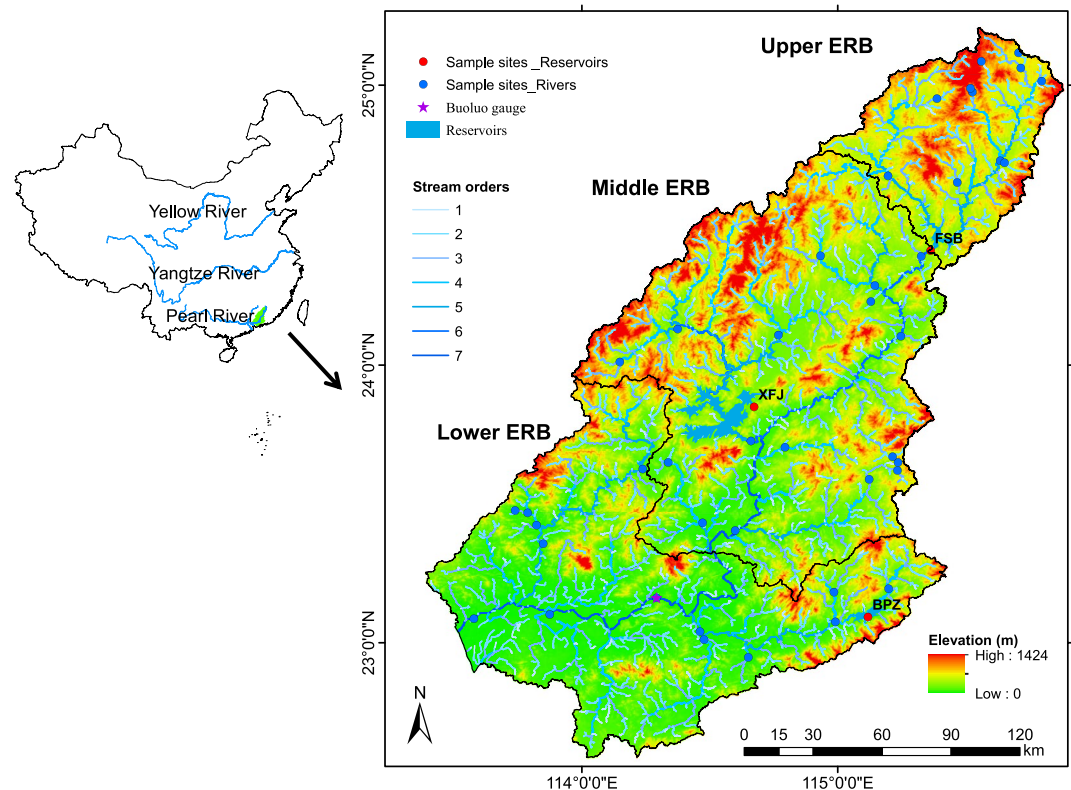


**Figure 1.** Location map of the East River Basin and sampling sites. Blue dots denote sampling sites in rivers, and red dots represent sampling sites in three large reservoirs, namely Baipenzhu (BPZ), Xinfengjiang (XFJ), and Fengshuba (FSB). Sampling sites were visited during five rounds of field campaigns from December 2018 to October 2019, including two (December and October) during the dry season (October–March) and three (April, July, and August) during the wet season (April–September).

precipitation is high and with substantial seasonal variability. The multi-annual average precipitation is about 1,800 mm, of which 80% falls in the wet season from April to September (B. Liu et al., 2021). The multi-annual average water discharge at the Boluo Hydrological Gauge, the lowermost gauge of the East River mainstem channel, is  $2.37 \times 10^{10} \text{ m}^3 \text{ yr}^{-1}$ , and about 80%–90% of the discharge is transported during the wet season (Y. D. Chen et al., 2011; S. Zhang et al., 2008). Because of sufficient precipitation, vegetation is dominated by highly diverse evergreen forests of broad-leaved and needle-leaved species (Q. Chen et al., 2013; Y. Ran et al., 2012). The ERB has experienced strong impacts from human activities. Rapid economic growth in the past decades has substantially accelerated the expansion of urban areas, especially in the Middle and Lower ERB (Deng & Chen, 2020), but forest and cropland are still the primary land use types. There are also three large reservoirs in the catchment (Figure 1) built from the 1960s to the 1980s, which could affect the hydrology of the East River.

## 2.2. Calculation of Water Surface Area

Water surface area (SA) needed for  $\text{CO}_2$  emissions estimates is often calculated based on river network and width databases, of which the accuracy is constrained by the spatial resolution of remote sensing imagery and the DEM used to create those databases (Allen & Pavelsky, 2018; Lehner et al., 2008). Since a great proportion of small rivers may not be included in the calculation because they are not identified in those databases, the water SA might have been significantly underestimated. Based on Sentinel-2 imagery with high spatial resolution and Multi-Error-Removed Improved-Terrain DEM, the river network in the ERB was extracted using the newly developed Remote Sensing Stream Burning (RSSB) tools and multi-spectral water index (MuWI) (Wang et al., 2018, 2021).

For the extraction, three main steps were adopted: water presence detection, spatial integration, and high-resolution extraction. First, water presence was identified using Sentinel-2 bands, and MuWI percentiles were then calculated

to build a composite image. We created the Sentinel-2 composite by calculating per-band, per-pixel percentiles of reflectance on the Google Earth Engine platform (Gorelick et al., 2017). The 50% percentile was used to reflect the average hydrological condition and to reduce uncertainties caused by intermittent acquisition time. In total, 1,513 Sentinel-2 images from 1 September 2015 to 1 September 2020 (<20% cloud cover) were used, including 948 images during the dry season (April–September) and 565 images during the wet season (October–March). A water map was then produced by identifying the water presence using a newly developed water index MuWI, a native 10 m water index on Sentinel-2 with lower commission error than Normalized Difference Water Index (NDWI) or Modified Normalized Difference Water Index (MNDWI) (Wang et al., 2021), according to:

$$\text{MuWI} = -4\text{ND}(2, 3) + 2\text{ND}(3, 8) + 2\text{ND}(3, 12) - \text{ND}(3, 11) \quad (1)$$

where,  $\text{ND}(i, j)$  is the normalized difference between Sentinel-2 *band i* and *band j*.

Second, the Multi-Error-Removed Improved-Terrain DEM (MERIT DEM) (Yamazaki et al., 2017) was integrated with the water index using the RSSB to inherit the high resolution from the imagery. We incorporated the MuWI-derived water map as the burnt layer into the DEM according to:

$$Z_{\text{burning}} = Z_{\text{base}} - \varphi \text{MuWI} \quad (2)$$

where,  $Z_{\text{base}}$  and  $Z_{\text{burning}}$  are elevations before and after the burning, respectively,  $\varphi$  represents the burning intensity parameter which is determined independently for each pixel according to:

$$\varphi = 10 + 10 \frac{A}{A_{95\%}} \quad (3)$$

where,  $A$  is the flow accumulation, and  $A_{95\%}$  is the 95% percentile of the flow accumulation in the entire basin. It can warrant a larger burning intensity for downstream floodplains and increase the accuracy of river network extraction. Notably, both water and land pixels have spatially continuous values in the MuWI-derived water map. As a result, it could reduce disconnection and parallel channels created by merely burning water pixels (Yamazaki et al., 2015, 2019).

Third, flow direction and accumulation were calculated through the common hydrological routing for the connected drainage network. We calculated flow direction and flow accumulation using the D8 algorithm (O'Callaghan & Mark, 1984), and applied a channelization threshold of 2.4 km<sup>2</sup>. Overall, seven Strahler stream orders were identified for the ERB (Figure 1), one order more than that in the HydroSHEDS database. This is consistent with the finding by Raymond et al. (2013) that the HydroSHEDS database might have overlooked one stream order. When comparing the total length of the stream network, our river length is substantially higher than the total length of six stream orders in the HydroSHEDS database, but about 20% lower than the combined length of seven stream orders calculated using the HydroSHEDS database and the relationship between stream orders and stream lengths (Table S3 in Supporting Information S1). The identified rivers were categorized, according to their stream orders, into small rivers (first- to third-order streams) and large rivers (fourth- to seventh-order streams).

The measured river widths for each Strahler stream order during field campaigns were used to determine the total SA of rivers. In total, there are 215 measurements from 43 sampling rivers. Since river width could vary greatly depending on the seasonally variable discharge, we calculated the average river widths for each stream orders during wet and dry season respectively and computed the water SA during those two seasons according to:

$$\text{SA} = \sum_{\text{SO}} (L \times W) \quad (4)$$

where,  $L$  and  $W$  are the total river length (m) and average river width (m) respectively, for a certain stream order during the wet or dry season.

We also compared the water SA calculated based on field-measured river width and the river width data obtained from the Global River Width from Landsat (GRWL) database (Allen & Pavelsky, 2018). We found that there was less than 4% difference in the annual average water SA between the two methods (Table S3 in Supporting Information S1). However, the difference between the two methods was 2.4% and 9.9% during the wet and dry seasons, respectively, indicating the importance of considering the seasonal change in water SA when calculating riverine CO<sub>2</sub> emissions.

### 2.3. Calculation of Annual CO<sub>2</sub> Efflux

Based on the riverine CO<sub>2</sub> partial pressure ( $p\text{CO}_2$ ) and gas transfer velocity ( $k$ ) data we collected in the ERB during five rounds of field campaigns from December 2018 to October 2019, including two (December and October) during the dry season (October–March) and three (April, July, and August) during the wet season (April–September), the total annual riverine CO<sub>2</sub> emissions was computed. Our earlier study in the ERB (B. Liu et al., 2021) showed that the spatial and temporal variability of CO<sub>2</sub> emissions mainly exhibited in three ways: (a) variability in CO<sub>2</sub> emissions among three sub-basins in the ERB (i.e., the Upper, Middle, and Lower ERB) was driven by changes in their land use covers; (b) spatial variability in CO<sub>2</sub> emissions between large downstream rivers (fourth- to seventh-order streams) and small headwater rivers (first- to third-order streams) was regulated by their differences in hydrological conditions and controls of riverine  $p\text{CO}_2$  and (c) temporal variability in CO<sub>2</sub> emissions between the wet and dry seasons was affected by seasonal changes in climate and hydrological conditions. Therefore, in each sub-basin, we calculated the areal CO<sub>2</sub> emission fluxes from each Strahler stream order according to:

$$F_{\text{CO}_2} = k \times k_0 \times (p\text{CO}_2^{\text{water}} - p\text{CO}_2^{\text{air}}) \quad (5)$$

where,  $k$  is the gas transfer velocity ( $\text{m d}^{-1}$ ),  $k_0$  is the solubility constants for CO<sub>2</sub> corrected for temperature and pressure ( $\text{mol L}^{-1} \text{atm}^{-1}$ ) from Weiss (1974),  $p\text{CO}_2^{\text{water}}$  is the mean riverine  $p\text{CO}_2$  for a given stream order within a given sub-basin, and  $p\text{CO}_2^{\text{air}}$  is average atmospheric  $p\text{CO}_2$ .

To calculate the areal CO<sub>2</sub> efflux in the wet and dry seasons, respectively, we use the average riverine  $p\text{CO}_2$  and atmospheric  $p\text{CO}_2$  of the two periods. In the wet and dry seasons, the average atmospheric  $p\text{CO}_2$  was 391 and 412  $\mu\text{atm}$ , respectively. A Li-850 CO<sub>2</sub>/H<sub>2</sub>O gas analyzer (Li-Cor, Inc, USA) was used in the field to measure both riverine and atmospheric  $p\text{CO}_2$ , and the headspace approach was adopted in the riverine  $p\text{CO}_2$  measurement (B. Liu et al., 2021). We used a 625 mL reagent bottle to collect 400 mL of water from ~10 cm below the surface, leaving 225 mL of space filled with ambient air as headspace. The bottle was then immediately sealed and shaken vigorously to create an equilibrium between the water and the CO<sub>2</sub> in the headspace (Hope et al., 1995). The bottle was connected to the calibrated Li-850 CO<sub>2</sub>/H<sub>2</sub>O gas analyzer, in which the equilibrated gas was measured. The measurements at each site were performed twice, and the average was then calculated. The difference between the two measurements was less than 5%, and the accuracy of Li-850 is within 1.5% of the reading. The original surface water  $p\text{CO}_2$  was determined based on  $p\text{CO}_2$  before and after the headspace equilibration (Text S1 in Supporting Information S1). In total, 215 measurements of  $p\text{CO}_2$  were conducted at 43 river sampling sites, including 129 and 86 measurements during the wet and dry seasons, respectively.

We estimated the  $k$  for each stream order based on 188 direct measurements, which were conducted using freely drifting chambers and an empirical model, Model 5 of Raymond et al. (2012):

$$k_{600} (\text{m d}^{-1}) = 2841 \times VS + 2.02 \quad (6)$$

Where,  $k_{600}$  is the standardized  $k$ , a Schmidt number of 600 by assigning the Schmidt number exponent a value of 2/3,  $V$  ( $\text{m s}^{-1}$ ) is the flow velocity measured in the field, and  $S$  (unitless) is the slope derived from DEM.

We compared the  $k$  calculated using Equation 5 and the modeled  $k$  (Equation 6). The results were highly consistent between the two methods, indicating that both are appropriate for estimating the  $k$  in the ERB (Figure S2a in Supporting Information S1). However, the average  $k$  at the sampling sites for small rivers (first- to third-order streams), either the measured or the modeled  $k$ , are significantly smaller than the modeled ones based on the average slope of each stream order (Figure S2b in Supporting Information S1). The underestimation may result from a sampling bias toward low-energy streams, since it is challenging to deploy freely drifting chambers in small and steep rivers. Therefore, the measured  $k$  was used for the calculation of areal CO<sub>2</sub> emission fluxes ( $F_{\text{CO}_2}$ ) in large rivers (fourth- to seventh-order streams), while the modeled  $k$  estimated based on the average slopes were used for the calculation of  $F_{\text{CO}_2}$  in small rivers (first- to third-order streams). To evaluate the error in  $F_{\text{CO}_2}$  calculations, we performed a Monte Carlo simulation for every stream order in every sub-basin (Text S2 in Supporting Information S1).

With  $F_{\text{CO}_2}$  in both the wet and dry seasons, we calculated total CO<sub>2</sub> emission fluxes ( $F_{\text{CO}_2}$ ,  $\text{Tg C yr}^{-1}$ ) by Strahler order within each of the three sub-basins according to:

$$F_{\text{CO}_2} = \sum_{\text{region}} \left[ \sum_{\text{SO}} (F_{\text{CO}_2} \times \text{SA} \times N \times 12 \div 10^{15}) \right] \quad (7)$$

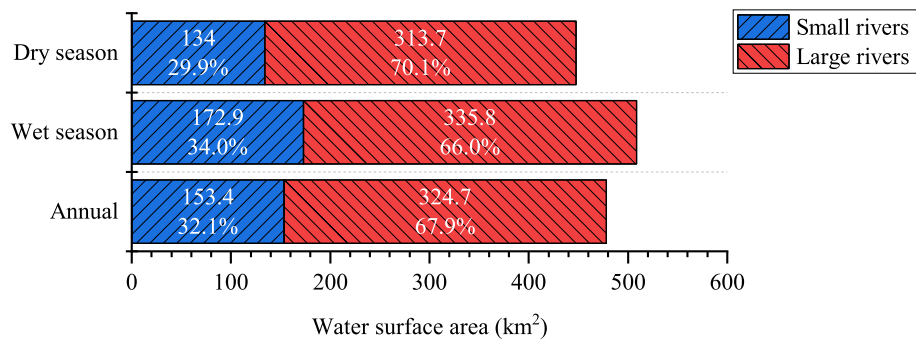


**Figure 2.** Seasonal changes in water surface area of small (first–third orders) and large (fourth–seventh orders) rivers in the East River basin.

where,  $FCO_2$  is the areal  $CO_2$  emission flux for a certain stream order within a given sub-basin during the wet or dry season,  $SA$  is the river water surface area ( $m^2$ ),  $N$  is the number of days in the wet or dry season, 12 is the molar mass of C ( $12\text{ g mol}^{-1}$ ), and  $10^{15}$  is the convertor from milligrams (mg) to teragrams (Tg). A sensitivity analysis was performed to assess the impact of different water SA and  $k$  calculation methods on the results of total  $CO_2$  emission estimations (Text S3 in Supporting Information S1).

To evaluate the impact of riverine  $CO_2$  emissions on regional carbon balance, we calculated the areal normalized riverine  $CO_2$  emissions ( $F_{nCO_2}$ ,  $g\text{ C m}^{-2}\text{ yr}^{-1}$ ) based on the  $F_{rCO_2}$  and the total area of the ERB ( $SA_r$ ) according to:

$$F_{nCO_2} = \frac{F_{rCO_2}}{SA_r} \quad (8)$$

The normalized areal ( $g\text{ C m}^{-2}\text{ yr}^{-1}$ ) and total ( $Tg\text{ C yr}^{-1}$ ) net ecosystem production (NEP) in the ERB was calculated using Net primary production (NPP) and heterotrophic soil respiration ( $R_h$ ) according to:

$$NEP = NPP - R_h \quad (9)$$

The MODIS/Terra net primary production yearly product in 2019 (Running & Zhao, 2021) and global soil and soil heterotrophic respiration data set (Stell et al., 2021) were used to calculate NPP and  $R_h$ , respectively.

### 3. Results

#### 3.1. Water Surface Area

With an annual average of  $478.2\text{ km}^2$ , the total water SA was  $508.7\text{ km}^2$  in the wet season, which was 13.6% higher than the  $447.7\text{ km}^2$  in the dry season (Figure 2). Small rivers (first- to third-order streams) exhibited more pronounced seasonal changes. The total SA of small rivers in the wet season was  $172.9\text{ km}^2$ , which was 29% higher than that in the dry season ( $134\text{ km}^2$ ). In comparison, the water SA of large rivers (fourth- to seventh-order streams) in the wet season was  $335.8\text{ km}^2$ , which was only 7.1% higher than that in the dry season ( $313.7\text{ km}^2$ ). Small rivers made up only 32.1% of the total SA, but the increase in SA of small rivers from the dry season to the wet season accounted for 63.7% of the seasonal area changes. This could substantially affect the seasonal pattern of riverine  $CO_2$  emissions.

#### 3.2. $CO_2$ Emissions From Rivers

The  $CO_2$  emissions from small rivers was considerably higher than that from large rivers. The average areal  $CO_2$  fluxes of small rivers were  $1,106 \pm 911\text{ mmol m}^{-2}\text{ d}^{-1}$ , about six times higher than the  $184 \pm 160\text{ mmol m}^{-2}\text{ d}^{-1}$  in large rivers (Table 1). As a result, small rivers contributed to more than 70% of the total  $CO_2$  emission fluxes (Figure 3), although they only accounted for about 30% of the total river SA. In contrast,

**Table 1**  
Seasonal Variations of Areal  $CO_2$  Fluxes in the East River Basin (ERB) and Three Sub-Basins

River basins	Stream size	Areal $CO_2$ flux ( $mmol\text{ m}^{-2}\text{ d}^{-1}$ )		
		Wet season	Dry season	Average
ERB	Small	$1,331 \pm 1,134$	$816 \pm 739$	$1,106 \pm 911$
	Large	$227 \pm 202$	$138 \pm 120$	$184 \pm 160$
Lower ERB	Small	$1,607 \pm 1,091$	$978 \pm 875$	$1,332 \pm 997$
	Large	$294 \pm 230$	$160 \pm 134$	$229 \pm 184$
Middle ERB	Small	$1,370 \pm 1,036$	$847 \pm 722$	$1,141 \pm 899$
	Large	$167 \pm 97$	$124 \pm 107$	$146 \pm 102$
Upper ERB	Small	$400 \pm 813$	$253 \pm 155$	$335 \pm 524$
	Large	$134 \pm 272$	$72 \pm 67$	$105 \pm 175$

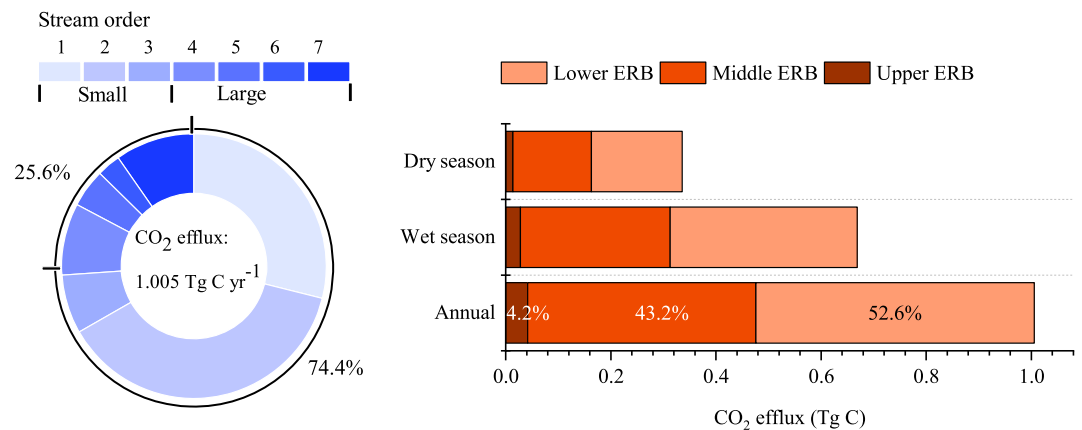


**Figure 3.** Comparison of CO<sub>2</sub> emissions from different Strahler order streams and three sub-basins in the ERB. (Left) relative importance of different Strahler order streams in riverine CO<sub>2</sub> evasion. Percentage contributions are given for small (first–third orders) and large (fourth–seventh orders) streams. (Right) seasonal variations in the contribution of Lower, Middle, and Upper ERB to total CO<sub>2</sub> efflux.

the large rivers, which accounted for around 70% of the total SA, were responsible for less than 30% of the total CO<sub>2</sub> emissions (Figure 3). The first- and second-order streams, responsible for 29.1% and 38.1% of the total emissions, respectively, were two major contributors. In comparison, none of the other stream orders contributed to more than 10% of the total emission fluxes.

Moreover, the Lower and Middle ERB, two heavily human-impacted sub-basins, were the primary sources of riverine CO<sub>2</sub> emissions. For example, the areal CO<sub>2</sub> emission fluxes were  $1,067 \pm 1,092$  and  $1,369 \pm 1,036$  mmol m<sup>-2</sup> d<sup>-1</sup> for small rivers in the Lower and Middle ERB, respectively, which were more than three times higher than that in the Upper ERB ( $400 \pm 813$  mmol m<sup>-2</sup> d<sup>-1</sup>) (Table 1). In total, the East River had annually emitted 1.005 Tg C (0.55–1.68 Tg C, Text S3 in Supporting Information S1) of CO<sub>2</sub>, of which 0.529 Tg C was from the Lower ERB, and 0.434 Tg was from the Middle ERB, making up 52.7% and 43.2% of the total emission fluxes, respectively (Figure 3). In comparison, the Upper ERB emitted only 0.042 Tg C of CO<sub>2</sub>, which was about 4.3% of the total annual fluxes (Figure 3).

In addition, the CO<sub>2</sub> emissions in the ERB showed significant seasonal variations. The areal CO<sub>2</sub> flux was  $1,331 \pm 1,134$  and  $227 \pm 202$  mmol m<sup>-2</sup> d<sup>-1</sup> for small and large rivers, respectively, during the wet season (Table 1), which was 83.9% and 64.5% higher than that during the dry season ( $816 \pm 739$  and  $138 \pm 120$ , respectively, for small and large rivers). Similar seasonal variations had also been observed in all the three sub-basins. For example, the areal CO<sub>2</sub> flux was  $1,607 \pm 1,091$  and  $294 \pm 230$  mmol m<sup>-2</sup> d<sup>-1</sup> for small and large rivers, respectively, in the Lower ERB, which were 64.3% and 83.8% higher than that during the dry season ( $978 \pm 875$  and  $160 \pm 134$  mmol m<sup>-2</sup> d<sup>-1</sup> for small and large rivers, respectively) (Table 1). As a result, CO<sub>2</sub> emission fluxes during the wet season accounted for 66.6% of the total annual CO<sub>2</sub> emission fluxes.

### 3.3. NEP and Normalized FCO<sub>2</sub>

The annual NEP was estimated to be 18.64 Tg C for the ERB (Figure 4b). The river networks emitted 1.005 Tg C yr<sup>-1</sup> accounting for 5.4% of the NEP. For the three sub-basins, riverine CO<sub>2</sub> emissions in the Lower ERB had the greatest offsetting effect on terrestrial ecosystem C fixation. Even though the areal NEP in the Lower ERB of 387 g C m<sup>-2</sup> yr<sup>-1</sup> was significantly lower than that in the Middle ERB (672.1 g C m<sup>-2</sup> yr<sup>-1</sup>) and the Upper ERB (621.8 g C m<sup>-2</sup> yr<sup>-1</sup>), the highest rate of riverine CO<sub>2</sub> emissions had been observed (Figure 4a). The areal normalized riverine CO<sub>2</sub> emission rate was 39.4 g C m<sup>-2</sup> yr<sup>-1</sup> for the Lower ERB, which was 42.8% and 303% higher than that in the Middle ERB and Upper ERB, respectively. As a result, riverine CO<sub>2</sub> emissions accounted for 10.6% of the NEP in the Lower ERB, but only 4.1% and 1.5% of the terrestrial NEP in the Middle ERB and Upper ERB, respectively.

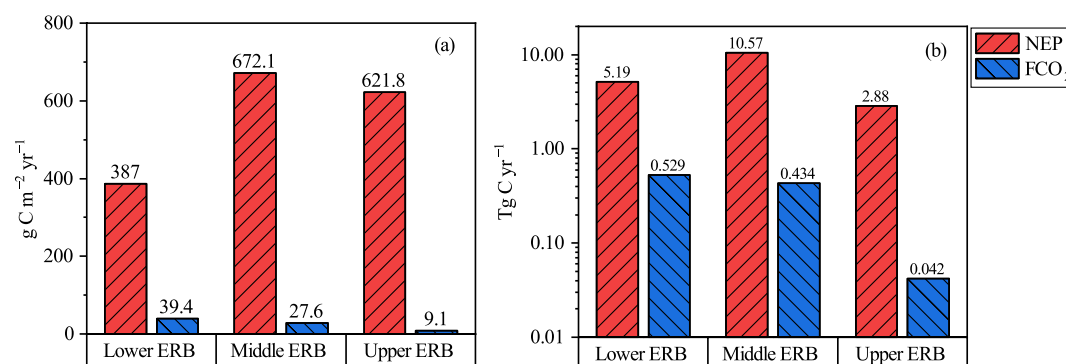


**Figure 4.** Comparison of CO<sub>2</sub> emissions from the three sub-basins of the East River Basin. (a) Areal normalized net ecosystem production (NEP) and FCO<sub>2</sub>, (b) Annual NEP and FCO<sub>2</sub>.

## 4. Discussions

### 4.1. Importance of Small Rivers in CO<sub>2</sub> Emission Estimates

This study further stresses the importance of small rivers in riverine CO<sub>2</sub> emissions, although their contribution is still subject to great uncertainty (Lauerwald et al., 2015; Marx et al., 2017; Raymond et al., 2013). In the ERB, small rivers are major contributors that generate over 70% of the total CO<sub>2</sub> emissions (Figure 3). The high emission contribution is attributable to two factors: a water SA comparable to that of large rivers and a substantially higher areal CO<sub>2</sub> emission flux. Because of the sufficient precipitation and dominant hilly topography in the river basin, the East River is a complex river network comprising extensive small rivers (Figure 1). The estimated length of small rivers is 17,831 km, accounting for about 90% of the total stream length (Table S3 in Supporting Information S1). As a result, small rivers, even though much smaller in size, not only account for 32.1% of the total river SA (Figure 2) but also contribute a disproportionate 74.4% of the total riverine CO<sub>2</sub> emissions (Figure 3). This is consistent with the finding that in mountainous regions where small rivers were widely developed, the contribution of first-order rivers could exceed 40% (Crawford et al., 2015; Schelker et al., 2016). Strong CO<sub>2</sub> emissions from small rivers have also been reported in tropical African rivers, where first- to third-order streams can contribute to 83% of the total CO<sub>2</sub> emissions (Mwanake et al., 2022).

High areal CO<sub>2</sub> efflux is the primary factor that causes the strong CO<sub>2</sub> emissions from small rivers. The average areal CO<sub>2</sub> emission flux for small rivers is  $1,106 \pm 911$  mmol m<sup>-2</sup> d<sup>-1</sup>, five times higher than the  $184 \pm 160$  mmol m<sup>-2</sup> d<sup>-1</sup> for large rivers (Table 1). However, small rivers in the ERB tend to have a relatively lower *p*CO<sub>2</sub> which is about 56.8% of that in large rivers (Table S7 in Supporting Information S1). This contradicts the understanding that strong CO<sub>2</sub> emissions in small rivers are usually associated with high *p*CO<sub>2</sub> and *k* (Butman & Raymond, 2011), and riverine CO<sub>2</sub> emissions may decrease as stream order increases because of lower *p*CO<sub>2</sub> and *k* in those high-order streams (Denfeld et al., 2013). The absence of high *p*CO<sub>2</sub> could result from the lack of C supply from the surrounding landscape. High *p*CO<sub>2</sub> in small rivers are typically derived from two sources, including groundwater carrying inorganic C originated from soils and in-stream decomposition of terrestrial organic C (Bernal et al., 2022; Duvert et al., 2018; Marx et al., 2017). In the ERB, groundwater CO<sub>2</sub> input could be substantially diluted due to extensive precipitation in this watershed (B. Liu et al., 2021), implying that in-stream metabolism could be the key mechanic controlling the *p*CO<sub>2</sub> dynamics in small rivers. However, due to the short water residence time induced by shorter river lengths and steep river channels, organic matter inputs from surrounding landscapes could not have enough time to decompose (Hotchkiss et al., 2015; S. Li et al., 2018) and would not be able to support a high *p*CO<sub>2</sub> in small rivers. In addition, wetland, known as a reliable C source for rivers (Abril & Borges, 2019), accounts for less than 1% of the total area of the ERB (Figure S5 in Supporting Information S1). Therefore, a considerable proportion of terrestrial C could not be converted into a more labile form in wetlands before entering the river network (Algesten et al., 2004; Moustapha et al., 2021), restricting the in-stream decomposition of terrestrial C.

Instead, the high CO<sub>2</sub> emissions from the small rivers in the ERB are mainly due to the high *k* which is controlled by the topological and hydrological conditions. Small rivers in the ERB tend to have steep river channels because of the prevailing hilly topography. The average slopes for first- to third-order streams are 5.2–22.5‰, which are



substantially greater than the 0.16–1.6‰ in large rivers (Table S4 in Supporting Information S1). Overall higher flow velocities were also observed in small rivers (0.57–0.83 and 0.34–0.61 m s<sup>-1</sup> during the wet and dry season, respectively) compared with that in large rivers (0.18–0.48 and 0.11–0.45 m s<sup>-1</sup>) (Table S4 in Supporting Information S1). As a result, the  $k$  is 63, 27.5, and 11.9 m d<sup>-1</sup> for first- to third-order streams during the wet season, respectively, which is an order of magnitude higher than that in large rivers (2.24–5.58 m d<sup>-1</sup>) (Figure S2 in Supporting Information S1). Even without high  $p\text{CO}_2$ ,  $\text{FCO}_2$  in small rivers could be six-fold higher than in large rivers (Table 1). The combination of low  $p\text{CO}_2$  and high  $k$  (Figure S6 in Supporting Information S1) has also been observed in other small mountainous rivers (Crawford et al., 2015; Schelker et al., 2016). Although steep slopes in mountainous streams could lead to low  $p\text{CO}_2$  (Rocher-Ros et al., 2019), the accompanying high  $k$  could eventually contribute to high  $\text{CO}_2$  emissions, outweighing the influence of low  $p\text{CO}_2$ . Therefore, although high  $\text{CO}_2$  emissions are widespread in small rivers, the underlying causes may differ greatly among regions. Considering the strong connection between small rivers and their surrounding landscapes, unraveling the response of small rivers to changing C inputs is crucial for a better understanding of the role of river networks in the basin-wide C cycle.

#### 4.2. Human Impacts on Riverine $\text{CO}_2$ Emissions

Substantially higher  $\text{CO}_2$  emissions have been observed in two sub-basins under intensified anthropogenic land cover changes. In the Middle and Lower ERB, where cropland and urban areas have replaced forest and become the dominant land cover type (Figure S5 in Supporting Information S1), the  $\text{FCO}_2$  are more than twice that in the forest-dominated Upper ERB (Table 1). The Middle ERB has the highest percentage of cropland cover, which accounts for 49% of the total area (Figure S5 in Supporting Information S1). Compared with forests, croplands are more vulnerable to soil erosion, thereby causing more terrestrial C transfer from land to rivers (Borges et al., 2018). Meanwhile, intensified agricultural practices could also promote the decomposition of soil organic matter and increase the concentration of  $\text{CO}_2$  and labile DOC in the soils, which could greatly enhance riverine  $p\text{CO}_2$  and  $\text{CO}_2$  emissions after entering river networks (Lambert et al., 2017; X. Li et al., 2019). The Lower ERB is where most major cities in the ERB are located. The urban area accounts for 17% of the total area of the Lower ERB, which is about twice that of the Middle ERB (8%) and eight times higher than that of the Upper ERB (2%) (Figure S5 in Supporting Information S1). The wastewater input with high organic matter concentrations from urban areas could enhance the in-stream decomposition and contribute to an increase in riverine  $p\text{CO}_2$  and  $\text{CO}_2$  emissions (Marescaux et al., 2018; Xuan et al., 2020; Yoon et al., 2017; W. Zhang et al., 2021). By interfering with the land use cover, human activity could alter the amount and form of C transported from terrestrial ecosystems to river networks, thereby changing the intensity of riverine  $\text{CO}_2$  emissions (Borges et al., 2018). Considering the intensification of land use change globally (Winkler et al., 2021), it is necessary to illustrate the impact of human activities when analyzing the controls of riverine  $\text{CO}_2$  emissions.

Riverine  $\text{CO}_2$  emissions are also a crucial component of the basin-wide C balance. It can offset the terrestrial NEP, thus reducing the C sequestration capacity of terrestrial ecosystems (Duvert et al., 2020; L. Ran et al., 2022). Meanwhile, anthropogenic land use changes can affect the NEP by altering land cover types (Xu et al., 2017) and the C budget by disturbing riverine  $\text{CO}_2$  emissions (Borges et al., 2018). The  $\text{FCO}_2$  to NEP ratios were 10.6% and 4.1% for the Lower and Middle ERB, respectively, which were six and three times higher than the 1.5% in the forest-dominated Upper ERB. For the Lower ERB, the highest NEP offsetting is the result of the lowest NEP (387 g C m<sup>-2</sup> yr<sup>-1</sup>) and highest  $\text{FCO}_2$  caused by urbanization and deforestation. In comparison, the terrestrial NEP was 672.1 g C m<sup>-2</sup> yr<sup>-1</sup> in the Middle ERB, even higher than the 621.8 g C m<sup>-2</sup> yr<sup>-1</sup> in the forest-dominated Upper ERB. This suggests that instead of directly reducing the terrestrial ecosystem productivity, land use change from forest to cropland has weakened the C sink of the terrestrial ecosystems mainly by enhancing the land-to-river C transport and riverine  $\text{CO}_2$  emissions. Notably, the  $\text{FCO}_2$  to NEP ratio in the ERB is relatively low compared with other river basins, considering riverine  $\text{CO}_2$  emissions could offset 60% of NEP globally (S. Liu et al., 2022). It suggests that subtropical terrestrial ecosystems like ERB are essential C sinks even when their C fixation capacities have been weakened by human disturbance. Therefore, exploring the human impacts on land-to-river C transport and riverine  $\text{CO}_2$  emissions is strongly needed to elucidate how human activities affect the C sink of terrestrial ecosystems and the C budget in a river basin.

By changing hydrological conditions and water SA, dam operation has modified and complicated  $\text{CO}_2$  emissions from the river networks (Deemer et al., 2016; Ollivier et al., 2019). However, reservoirs in the ERB only play a

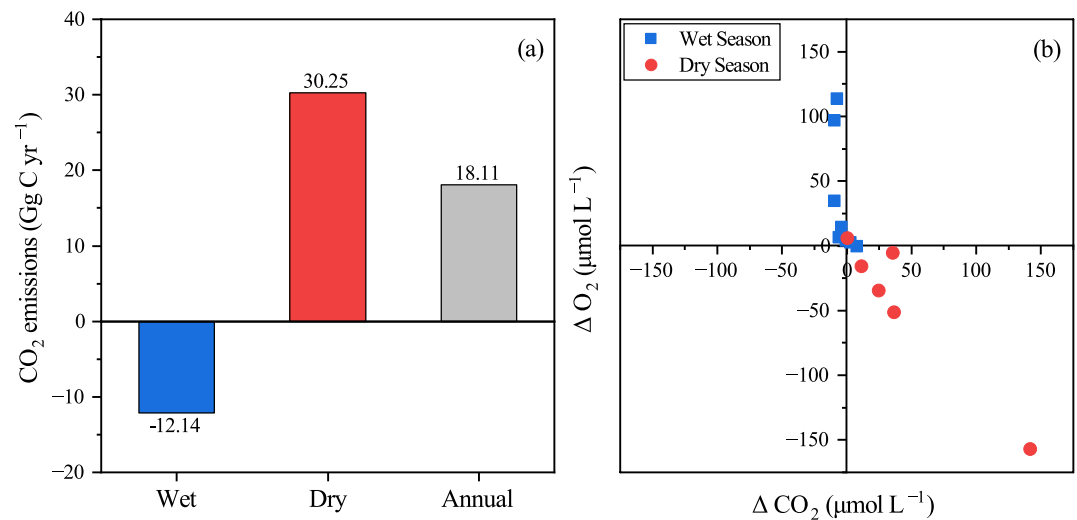


**Figure 5.** (a) Seasonal and annual CO<sub>2</sub> fluxes at the reservoir-air interface. Values less than zero indicate C uptake from the atmosphere, and values greater than zero indicate C emissions. (b) The relationship between ΔCO<sub>2</sub> and ΔO<sub>2</sub> in the three reservoirs. ΔCO<sub>2</sub> and ΔO<sub>2</sub> are the difference between the measured concentrations of gases (CO<sub>2</sub> and O<sub>2</sub>, respectively) in water and their calculated concentrations in equilibrium with the atmosphere (Stets et al., 2017). Points greater than zero are oversaturated, and points less than zero are undersaturated.

minor role in the CO<sub>2</sub> emissions from the river networks (Text S2 in Supporting Information S1). The water SA of these reservoirs (377.5 km<sup>2</sup>) is comparable to that of the rivers (478.2 km<sup>2</sup>). However, the annual CO<sub>2</sub> efflux from the three large reservoirs is only 18.1 Gg C, less than 2% of the total riverine CO<sub>2</sub> emission fluxes (Figure 5a). This is expected since we have observed relatively low *k* and *p*CO<sub>2</sub> in the reservoirs (Figure S4 in Supporting Information S1). Due to the lentic environment, reservoirs have a relatively low *k* ranging from 0.98 to 6.02 m d<sup>-1</sup> with a mean of 2.76 m d<sup>-1</sup>, which is similar to that in large rivers (Figure S2 in Supporting Information S1). Moreover, the seasonal variation of CO<sub>2</sub> emissions from the three large reservoirs differed from that in rivers. Instead of hotspots for CO<sub>2</sub> emissions, reservoirs in the ERB functioned as C sinks that uptake 12.14 Gg C yr<sup>-1</sup> from the atmosphere during the wet season (Figure 5a). The saturated dissolved oxygen (Figure 5b) in reservoirs during the wet season implies that C sink during wet season may result from enhanced primary production. Long water residence time due to dam impoundment combined with high temperature and intense solar radiation during the wet season have created a favorable condition for photosynthesis which leads to C uptake (Amaral et al., 2018; Crawford et al., 2016). Therefore, the construction of reservoirs in the ERB did not significantly increase the CO<sub>2</sub> emissions from the river networks. However, further research is warranted to understand its impact on the hydrological conditions upstream and downstream of the river and the lateral C transport, which will inevitably affect the C emissions from the river networks.

### 4.3. Riverine CO<sub>2</sub> Emission Estimation Complicated by Monsoons

Substantial seasonal differences in temperature and precipitation under subtropical monsoon climate could lead to pronounced seasonal variations of riverine CO<sub>2</sub> emissions from the ERB. Due to the larger water SA, higher *k* and *p*CO<sub>2</sub>, the CO<sub>2</sub> emission during the wet season (0.67 Tg C yr<sup>-1</sup>) was about twice that of the dry season (0.33 Tg C yr<sup>-1</sup>; Figure 3). Due to increased precipitation-induced discharge, the total river SA of the East River during the wet season was 508.7 km<sup>2</sup>, 13.6% higher than that during the dry season (447.7 km<sup>2</sup>; Figure 2). Particularly, the water SA of small rivers, the major contributors to riverine CO<sub>2</sub> emissions, increased by about 20% from the dry season to the wet season. This suggests that ignoring the seasonal changes in water SA could lead to an underestimation of seasonal variation in CO<sub>2</sub> emissions and its total annual amount (Mwanake et al., 2022). However, such neglect was common when calculating riverine CO<sub>2</sub> emissions based on river width databases (Lauerwald et al., 2015). Currently, global river width datasets struggle to offer seasonal river widths for CO<sub>2</sub> emission estimations due to the low resolution of the satellite images (Allen & Pavelsky, 2018). Even though the total SA calculated from databases might not be that different from the one calculated based on field-measured data (Table S3 in Supporting Information S1), it may result in an underesti-

mation of seasonal differences and the total riverine CO<sub>2</sub> emission fluxes. Therefore, it is important to consider the impact of seasonal river surface changes on regional riverine CO<sub>2</sub> emission estimates, especially for small rivers (Mwanake et al., 2022).

Monsoon-induced high discharge during the wet season could also affect the accuracy of  $k$  estimation. During the wet season, the measured  $k$  in large rivers was more than 90% greater than that during the dry season. In comparison, the variation in modeled  $k$  was only 10%–40% between wet and dry seasons (Table S4 in Supporting Information S1). It is possible that the Raymond et al. (2012) approach has underestimated the impact of flow velocity on  $k$  while overvalued the impact of the slope. As a result, a 30% underestimation of the wet season  $k$  has been observed relative to the measured  $k$  in large rivers. In comparison, there is a 10%–20% overestimation of the wet season  $k$  in small rivers (Figure S2 in Supporting Information S1). This implies that, due to the comparatively low slope, the contribution of increased flow velocity on  $k$  during the wet season in large rivers has been under-rated. This may result from the under-sampling during flood events when developing the  $k$  model (Raymond et al., 2012, 2013). The  $k$  could increase disproportionately under large discharge conditions, especially during flood events (Almeida et al., 2017; Long et al., 2015). In the East River, the  $k$  could be one order of magnitude higher during the wet season than during the dry season. Therefore, the lack of sampling during large discharge conditions could lead to underestimated  $k$ . The inclusion of measured  $k$  during flood events is crucial for more accurate CO<sub>2</sub> emission estimates.

## 5. Conclusions

The spatial and temporal characteristics of riverine CO<sub>2</sub> emissions vary greatly among rivers, making it hard for quantitative evaluation. In the ERB, the subtropical monsoon climate, hilly topography, and diverse human activities all influence CO<sub>2</sub> emissions from the river network. We calculated total CO<sub>2</sub> emission fluxes by Strahler stream order within each of the three sub-basins during the wet and dry seasons and examined the impacts of those three controlling factors. We found that small rivers are major contributors to riverine CO<sub>2</sub> emissions. Despite accounting for just 32.1% of the total river SA, they contribute a disproportionate 74.4% of the total CO<sub>2</sub> emissions. However, small rivers in the ERB tend to have high areal CO<sub>2</sub> efflux but relatively lower  $p$ CO<sub>2</sub>, which suggests that large CO<sub>2</sub> fluxes from the small rivers mainly result from the high  $k$  that is controlled by the topological and hydrological conditions.

We also assessed the human impacts on riverine CO<sub>2</sub> emissions in the Lower and Middle ERB, where urban and cropland predominate. The FCO<sub>2</sub> in those two sub-basins are more than double those in the forest-dominated Upper ERB. The anthropogenic land use changes could also affect the contribution of riverine CO<sub>2</sub> emissions to regional C balance. Normalized areal riverine CO<sub>2</sub> fluxes in the urban- and cropland-dominated Middle and Lower ERB (27.6 and 39.4 g C m<sup>-2</sup> yr<sup>-1</sup>), which offset the NEP by 10.6% and 4.1%, respectively, were two and three times higher than the 9.1 g C m<sup>-2</sup> yr<sup>-1</sup> in the forest dominated Upper ERB. Reservoirs, which we expected to substantially alter the aquatic CO<sub>2</sub> emissions, only emitted 18.11 Gg C yr<sup>-1</sup>, less than 2% of CO<sub>2</sub> fluxes from rivers. In addition, seasonal fluctuations in discharge due to monsoon-induced precipitation variation may impair the accuracy of CO<sub>2</sub> emission estimates since variations in water SA and  $k$  caused by seasonal discharge changes are underrepresented in existing databases and models. It implies that increasing field measurements of river width and  $k$  is crucial for more accurate CO<sub>2</sub> emission estimates, especially in regions with substantial seasonal precipitation changes. Our study has illustrated how monsoon climate and land use in the ERB control riverine CO<sub>2</sub> emissions. We have also evaluated the contribution of small rivers to riverine CO<sub>2</sub> emissions, which could provide valuable insights into the role of small rivers in the basin-wide C cycle.

## Conflict of Interest

The authors declare no conflicts of interest relevant to this study.

## Data Availability Statement

All data necessary to reproduce the reported finding are available at <https://doi.org/10.25442/hku.13416281.v2>.

### Acknowledgments

This study was funded by the Research Grants Council of Hong Kong (Grants 17300619 and 17300621) and National Natural Science Foundation of China (Grant 42222062).

### References

- Abril, G., & Borges, A. (2019). Ideas and perspectives: Carbon leaks from flooded land: Do we need to replumb the inland water active pipe? *Biogeosciences*, *16*(3), 769–784. <https://doi.org/10.5194/bg-16-769-2019>
- Algesten, G., Sobek, S., Bergström, A. K., Ågren, A., Tranvik, L. J., & Jansson, M. (2004). Role of lakes for organic carbon cycling in the boreal zone. *Global Change Biology*, *10*(1), 141–147. <https://doi.org/10.1111/j.1365-2486.2003.00721.x>
- Allen, G. H., & Pavelsky, T. M. (2018). Global extent of rivers and streams. *Science*, *361*(6402), 585–588. <https://doi.org/10.1126/science.aat0636>
- Almeida, R. M., Pacheco, F. S., Barros, N., Rosi, E., & Roland, F. (2017). Extreme floods increase CO<sub>2</sub> outgassing from a large Amazonian river. *Limnology & Oceanography*, *62*(3), 989–999. <https://doi.org/10.1002/lno.10480>
- Amaral, J. H. F., Borges, A. V., Melack, J. M., Sarmento, H., Barbosa, P. M., Kasper, D., et al. (2018). Influence of plankton metabolism and mixing depth on CO<sub>2</sub> dynamics in an Amazon floodplain lake. *Science of the Total Environment*, *630*, 1381–1393. <https://doi.org/10.1016/j.scitotenv.2018.02.331>
- Battin, T. J., Luysaert, S., Kaplan, L. A., Aufdenkampe, A. K., Richter, A., & Tranvik, L. J. (2009). The boundless carbon cycle. *Nature Geoscience*, *2*(9), 598–600. <https://doi.org/10.1038/ngeo618>
- Bernal, S., Cohen, M. J., Ledesma, J. L. J., Kirk, L., Martí, E., & Lupon, A. (2022). Stream metabolism sources a large fraction of carbon dioxide to the atmosphere in two hydrologically contrasting headwater streams. *Limnology & Oceanography*, *67*(12), 2621–2634. <https://doi.org/10.1002/lno.12226>
- Borges, A. V., Darchambeau, F., Lambert, T., Bouillon, S., Morana, C., Brouyere, S., et al. (2018). Effects of agricultural land use on fluvial carbon dioxide, methane and nitrous oxide concentrations in a large European river, the Meuse (Belgium). *Science of the Total Environment*, *610–611*, 342–355. <https://doi.org/10.1016/j.scitotenv.2017.08.047>
- Borges, A. V., Darchambeau, F., Lambert, T., Morana, C., Allen, G. H., Tambwe, E., et al. (2019). Variations in dissolved greenhouse gases (CO<sub>2</sub>, CH<sub>4</sub>, N<sub>2</sub>O) in the Congo River network overwhelmingly driven by fluvial-wetland connectivity. *Biogeosciences*, *16*(19), 3801–3834. <https://doi.org/10.5194/bg-16-3801-2019>
- Borges, A. V., Darchambeau, F., Teodoru, C. R., Marwick, T. R., Tamoo, F., Geeraert, N., et al. (2015). Globally significant greenhouse-gas emissions from African inland waters. *Nature Geoscience*, *8*(8), 637–642. <https://doi.org/10.1038/ngeo2486>
- Butman, D., & Raymond, P. A. (2011). Significant efflux of carbon dioxide from streams and rivers in the United States. *Nature Geoscience*, *4*(12), 839–842. <https://doi.org/10.1038/ngeo1294>
- Chen, Q., Xu, W., Li, S., Fu, S., & Yan, J. (2013). Aboveground biomass and corresponding carbon sequestration ability of four major forest types in south China. *Chinese Science Bulletin*, *58*(13), 1551–1557. <https://doi.org/10.1007/s11434-012-5100-8>
- Chen, Y. D., Zhang, Q., Lu, X., Zhang, S., & Zhang, Z. (2011). Precipitation variability (1956–2002) in the Dongjiang River (Zhujiang River basin, China) and associated large-scale circulation. *Quaternary International*, *244*(2), 130–137. <https://doi.org/10.1016/j.quaint.2010.08.013>
- Chi, J., Nilsson, M. B., Laudon, H., Lindroth, A., Wallerman, J., Fransson, J. E. S., et al. (2020). The net landscape carbon balance—Integrating terrestrial and aquatic carbon fluxes in a managed boreal forest landscape in Sweden. *Global Change Biology*, *26*(4), 2353–2367. <https://doi.org/10.1111/gcb.14983>
- Clow, D. W., Striegl, R. G., & Dornblaser, M. M. (2021). Spatiotemporal dynamics of CO<sub>2</sub> gas exchange from headwater mountain streams. *Journal of Geophysical Research: Biogeosciences*, *126*(9), e2021JG006509. <https://doi.org/10.1029/2021JG006509>
- Cole, J. J., Prairie, Y. T., Caraco, N. F., McDowell, W. H., Tranvik, L. J., Striegl, R. G., et al. (2007). Plumbing the global carbon cycle: Integrating inland waters into the terrestrial carbon budget. *Ecosystems*, *10*(1), 172–185. <https://doi.org/10.1007/s10021-006-9013-8>
- Crawford, J. T., Dornblaser, M. M., Stanley, E. H., Clow, D. W., & Striegl, R. G. (2015). Source limitation of carbon gas emissions in high-elevation mountain streams and lakes. *Journal of Geophysical Research: Biogeosciences*, *120*(5), 952–964. <https://doi.org/10.1002/2014jg002861>
- Crawford, J. T., Loken, L. C., Stanley, E. H., Stets, E. G., Dornblaser, M. M., & Striegl, R. G. (2016). Basin scale controls on CO<sub>2</sub> and CH<sub>4</sub> emissions from the Upper Mississippi River. *Geophysical Research Letters*, *43*(5), 1973–1979. <https://doi.org/10.1002/2015GL067599>
- Deemer, B. R., Harrison, J. A., Li, S., Beaulieu, J. J., DelSontro, T., Barros, N., et al. (2016). Greenhouse gas emissions from reservoir water surfaces: A new global synthesis. *BioScience*, *66*(11), 949–964. <https://doi.org/10.1093/biosci/biw117>
- Deirmendjian, L., & Abril, G. (2018). Carbon dioxide degassing at the groundwater-stream-atmosphere interface: Isotopic equilibration and hydrological mass balance in a sandy watershed. *Journal of Hydrology*, *558*, 129–143. <https://doi.org/10.1016/j.jhydrol.2018.01.003>
- Denfeld, B. A., Frey, K. E., Sobczak, W. V., Mann, P. J., & Holmes, R. M. (2013). Summer CO<sub>2</sub> evasion from streams and rivers in the Kolyma River basin, north-east Siberia. *Polar Research*, *32*(1), 19704. <https://doi.org/10.3402/polar.v32i0.19704>
- Deng, X., & Chen, Y. (2020). Land use change and its driving mechanism in Dongjiang River basin from 1990 to 2018. *Bulletin of Soil and Water Conservation*, *40*, 236–242. <https://doi.org/10.13961/j.cnki.stbctb.2020.06.034>
- Drake, T. W., Raymond, P. A., & Spencer, R. G. (2018). Terrestrial carbon inputs to inland waters: A current synthesis of estimates and uncertainty. *Limnology and Oceanography Letters*, *3*(3), 132–142. <https://doi.org/10.1002/lol2.10055>
- Drake, T. W., Van Oost, K., Barthel, M., Bauters, M., Hoyt, A. M., Podgorski, D. C., et al. (2019). Mobilization of aged and biolabile soil carbon by tropical deforestation. *Nature Geoscience*, *12*(7), 541–546. <https://doi.org/10.1038/s41561-019-0384-9>
- Duvert, C., Butman, D. E., Marx, A., Ribolzi, O., & Hutley, L. B. (2018). CO<sub>2</sub> evasion along streams driven by groundwater inputs and geomorphic controls. *Nature Geoscience*, *11*(11), 813–818. <https://doi.org/10.1038/s41561-018-0245-y>
- Duvert, C., Hutley, L. B., Beringer, J., Bird, M. I., Birkel, C., Maher, D. T., et al. (2020). Net landscape carbon balance of a tropical savanna: Relative importance of fire and aquatic export in offsetting terrestrial production. *Global Change Biology*, *26*(10), 5899–5913. <https://doi.org/10.1111/gcb.15287>
- Gallay, M., Mora, A., Martinez, J.-M., Gardel, A., Laraque, A., Sarrazin, M., et al. (2018). Dynamics and fluxes of organic carbon and nitrogen in two Guiana Shield river basins impacted by deforestation and mining activities. *Hydrological Processes*, *32*(1), 17–29. <https://doi.org/10.1002/hyp.11394>
- Gorelick, N., Hancher, M., Dixon, M., Ilyushchenko, S., Thau, D., & Moore, R. (2017). Google Earth Engine: Planetary-scale geospatial analysis for everyone. *Remote Sensing of Environment*, *202*, 18–27. <https://doi.org/10.1016/j.rse.2017.06.031>
- Gu, S., Li, S., & Santos, I. R. (2022). Anthropogenic land use substantially increases riverine CO<sub>2</sub> emissions. *Journal of Environmental Sciences*, *118*, 158–170. <https://doi.org/10.1016/j.jes.2021.12.040>
- Hope, D., Dawson, J. J. C., Cresser, M. S., & Billett, M. F. (1995). A method for measuring free CO<sub>2</sub> in upland streamwater using headspace analysis. *Journal of Hydrology*, *166*(1), 1–14. [https://doi.org/10.1016/0022-1694\(94\)02628-0](https://doi.org/10.1016/0022-1694(94)02628-0)
- Hotchkiss, E., Hall, R., Jr., Sponseller, R., Butman, D., Klaminder, J., Laudon, H., et al. (2015). Sources of and processes controlling CO<sub>2</sub> emissions change with the size of streams and rivers. *Nature Geoscience*, *8*(9), 696–699. <https://doi.org/10.1038/ngeo2507>

- Lambert, T., Bouillon, S., Darchambeau, F., Morana, C., Roland, F. A. E., Descy, J.-P., & Borges, A. V. (2017). Effects of human land use on the terrestrial and aquatic sources of fluvial organic matter in a temperate river basin (The Meuse River, Belgium). *Biogeochemistry*, *136*(2), 191–211. <https://doi.org/10.1007/s10533-017-0387-9>
- Lauerwald, R., Laruelle, G. G., Hartmann, J., Ciais, P., & Regnier, P. A. (2015). Spatial patterns in CO<sub>2</sub> evasion from the global river network. *Global Biogeochemical Cycles*, *29*(5), 534–554. <https://doi.org/10.1002/2014GB004941>
- Lauerwald, R., Regnier, P., Guenet, B., Friedlingstein, P., & Ciais, P. (2020). How simulations of the land carbon sink are biased by ignoring fluvial carbon transfers: A case study for the Amazon basin. *One Earth*, *3*(2), 226–236. <https://doi.org/10.1016/j.oneear.2020.07.009>
- Lehner, B., Verdin, K., & Jarvis, A. (2008). New global hydrography derived from spaceborne elevation data. *Eos, Transactions American Geophysical Union*, *89*(10), 93–94. <https://doi.org/10.1029/2008EO100001>
- Li, S., Ni, M., Mao, R., & Bush, R. T. (2018). Riverine CO<sub>2</sub> supersaturation and outgassing in a subtropical monsoonal mountainous area (Three Gorges Reservoir Region) of China. *Journal of Hydrology*, *558*, 460–469. <https://doi.org/10.1016/j.jhydrol.2018.01.057>
- Li, X., Xu, J., Shi, Z., & Li, R. (2019). Response of bacterial metabolic activity to the river discharge in the Pearl River estuary: Implication for CO<sub>2</sub> degassing fluxes. *Frontiers in Microbiology*, *10*(1026), 1026. <https://doi.org/10.3389/fmicb.2019.01026>
- Liu, B., Tian, M., Shih, K., Chan, C. N., Yang, X., & Ran, L. (2021). Spatial and temporal variability of pCO<sub>2</sub> and CO<sub>2</sub> emissions from the Dong River in south China. *Biogeosciences*, *18*(18), 5231–5245. <https://doi.org/10.5194/bg-18-5231-2021>
- Liu, S., Kuhn, C., Amatulli, G., Aho, K., Butman, D. E., Allen, G. H., et al. (2022). The importance of hydrology in routing terrestrial carbon to the atmosphere via global streams and rivers. *Proceedings of the National Academy of Sciences*, *119*(11), e2106322119. <https://doi.org/10.1073/pnas.2106322119>
- Long, H., Vihermaa, L., Waldron, S., Hoey, T., Quemin, S., & Newton, J. (2015). Hydraulics are a first-order control on CO<sub>2</sub> efflux from fluvial systems. *Journal of Geophysical Research: Biogeosciences*, *120*(10), 1912–1922. <https://doi.org/10.1002/2015JG002955>
- Marescaux, A., Thieu, V., & Garnier, J. (2018). Carbon dioxide, methane and nitrous oxide emissions from the human-impacted Seine watershed in France. *Science of the Total Environment*, *643*, 247–259. <https://doi.org/10.1016/j.scitotenv.2018.06.151>
- Marx, A., Dusek, J., Jankovec, J., Sanda, M., Vogel, T., van Geldern, R., et al. (2017). A review of CO<sub>2</sub> and associated carbon dynamics in headwater streams: A global perspective. *Reviews of Geophysics*, *55*(2), 560–585. <https://doi.org/10.1002/2016rg000547>
- Moustapha, M., Deirmendjian, L., Sebag, D., Braun, J. J., Audry, S., Ateba Bessa, H., et al. (2021). Partitioning carbon sources in a tropical watershed (Nyong River, Cameroon) between wetlands and terrestrial ecosystems—Do CO<sub>2</sub> emissions from tropical rivers offset the terrestrial carbon sink? *Biogeosciences Discussions*, *2021*, 1–30. <https://doi.org/10.5194/bg-2021-69>
- Mwanake, R. M., Gettel, G. M., Ishimwe, C., Wangari, E. G., Butterbach-Bahl, K., & Kiese, R. (2022). Basin-scale estimates of greenhouse gas emissions from the Mara River, Kenya: Importance of discharge, stream size, and land use/land cover. *Limnology & Oceanography*, *67*(8), 1776–1793. <https://doi.org/10.1002/lno.12166>
- O'Callaghan, J. F., & Mark, D. M. (1984). The extraction of drainage networks from digital elevation data. *Computer Vision, Graphics, and Image Processing*, *28*(3), 323–344. [https://doi.org/10.1016/s0734-189x\(84\)80011-0](https://doi.org/10.1016/s0734-189x(84)80011-0)
- Ollivier, Q. R., Maher, D. T., Pitfield, C., & Macreadie, P. I. (2019). Punching above their weight: Large release of greenhouse gases from small agricultural dams. *Global Change Biology*, *25*(2), 721–732. <https://doi.org/10.1111/gcb.14477>
- Ran, L., Butman, D. E., Battin, T. J., Yang, X., Tian, M., Duvert, C., et al. (2021). Substantial decrease in CO<sub>2</sub> emissions from Chinese inland waters due to global change. *Nature Communications*, *12*(1), 1730. <https://doi.org/10.1038/s41467-021-21926-6>
- Ran, L., Wang, X., Li, S., Zhou, Y., Xu, Y. J., Chan, C. N., et al. (2022). Integrating aquatic and terrestrial carbon fluxes to assess the net landscape carbon balance of a highly erodible semiarid catchment. *Journal of Geophysical Research: Biogeosciences*, *127*(3), e2021JG006765. <https://doi.org/10.1029/2021jg006765>
- Ran, Y., Li, X., Lu, L., & Li, Z. (2012). Large-scale land cover mapping with the integration of multi-source information based on the Dempster-Shafer theory. *International Journal of Geographical Information Science*, *26*(1), 169–191. <https://doi.org/10.1080/13658816.2011.577745>
- Raymond, P. A., Hartmann, J., Lauerwald, R., Sobek, S., McDonald, C., Hoover, M., et al. (2013). Global carbon dioxide emissions from inland waters. *Nature*, *503*(7476), 355–359. <https://doi.org/10.1038/nature12760>
- Raymond, P. A., Zappa, C. J., Butman, D., Bott, T. L., Potter, J., Mulholland, P., et al. (2012). Scaling the gas transfer velocity and hydraulic geometry in streams and small rivers. *Limnology and Oceanography: Fluids and Environments*, *2*(1), 41–53. <https://doi.org/10.1215/21573689-1597669>
- Regnier, P., Resplandy, L., Najjar, R. G., & Ciais, P. (2022). The land-to-ocean loops of the global carbon cycle. *Nature*, *603*(7901), 401–410. <https://doi.org/10.1038/s41586-021-04339-9>
- Rocher-Ros, G., Sponseller, R. A., Lidberg, W., Mörth, C. M., & Giesler, R. (2019). Landscape process domains drive patterns of CO<sub>2</sub> evasion from river networks. *Limnology and Oceanography Letters*, *4*(4), 87–95. <https://doi.org/10.1002/lol2.10108>
- Running, S., & Zhao, M. (2021). MODIS/terra net primary production gap-filled yearly L4 global 500 m SIN grid V061.
- Sawakuchi, H. O., Neu, V., Ward, N. D., Barros, M. D. L. C., Valerio, A. M., Gagne-Maynard, W., et al. (2017). Carbon dioxide emissions along the lower Amazon River. *Frontiers in Marine Science*, *4*(76), 76. <https://doi.org/10.3389/fmars.2017.00076>
- Schelker, J., Singer, G. A., Ulseth, A. J., Hengsberger, S., & Battin, T. J. (2016). CO<sub>2</sub> evasion from a steep, high gradient stream network: Importance of seasonal and diurnal variation in aquatic pCO<sub>2</sub> and gas transfer. *Limnology & Oceanography*, *61*(5), 1826–1838. <https://doi.org/10.1002/lno.10339>
- Schneider, C. L., Herrera, M., Raisle, M. L., Murray, A. R., Whitmore, K. M., Encalada, A. C., et al. (2020). Carbon dioxide (CO<sub>2</sub>) fluxes from terrestrial and aquatic environments in a high-altitude tropical catchment. *Journal of Geophysical Research: Biogeosciences*, *125*(8), e2020JG005844. <https://doi.org/10.1029/2020JG005844>
- Stell, E., Warner, D. L., Jian, J., Bond-Lamberty, B. P., & Vargas, R. (2021). Global gridded 1-km soil and soil heterotrophic respiration derived from SRDB v5. In *ORNL Distributed Active Archive Center*.
- Stets, E. G., Butman, D., McDonald, C. P., Stackpoole, S. M., DeGrandpre, M. D., & Striegl, R. G. (2017). Carbonate buffering and metabolic controls on carbon dioxide in rivers. *Global Biogeochemical Cycles*, *31*(4), 663–677. <https://doi.org/10.1002/2016gb005578>
- Wang, Z., Liu, J., Li, J., Meng, Y., Pokhrel, Y., & Zhang, H. (2021). Basin-scale high-resolution extraction of drainage networks using 10-m Sentinel-2 imagery. *Remote Sensing of Environment*, *255*, 112281. <https://doi.org/10.1016/j.rse.2020.112281>
- Wang, Z., Liu, J., Li, J., & Zhang, D. D. (2018). Multi-spectral water index (MuWI): A native 10-m multi-spectral water index for accurate water mapping on sentinel-2. *Remote Sensing*, *10*(10), 1643. <https://doi.org/10.3390/rs10101643>
- Weiss, R. F. (1974). Carbon dioxide in water and seawater: The solubility of a non-ideal gas. *Marine Chemistry*, *2*(3), 203–215. [https://doi.org/10.1016/0304-4203\(74\)90015-2](https://doi.org/10.1016/0304-4203(74)90015-2)
- Winkler, K., Fuchs, R., Rounsevell, M., & Herold, M. (2021). Global land use changes are four times greater than previously estimated. *Nature Communications*, *12*(1), 2501. <https://doi.org/10.1038/s41467-021-22702-2>
- Xu, X., Yang, G., Tan, Y., Tang, X., Jiang, H., Sun, X., et al. (2017). Impacts of land use changes on net ecosystem production in the Taihu Lake Basin of China from 1985 to 2010. *Journal of Geophysical Research: Biogeosciences*, *122*(3), 690–707. <https://doi.org/10.1002/2016jg003444>

- Xuan, Y., Cao, Y., Tang, C., & Li, M. (2020). Changes in dissolved inorganic carbon in river water due to urbanization revealed by hydrochemistry and carbon isotope in the Pearl River Delta, China. *Environmental Science and Pollution Research*, 27(19), 24542–24557. <https://doi.org/10.1007/s11356-020-08454-4>
- Yamazaki, D., Ikeshima, D., Sosa, J., Bates, P. D., Allen, G. H., & Pavelsky, T. M. (2019). MERIT hydro: A high-resolution global hydrography map based on latest topography dataset. *Water Resources Research*, 55(6), 5053–5073. <https://doi.org/10.1029/2019wr024873>
- Yamazaki, D., Ikeshima, D., Tawatari, R., Yamaguchi, T., O'Loughlin, F., Neal, J. C., et al. (2017). A high-accuracy map of global terrain elevations. *Geophysical Research Letters*, 44(11), 5844–5853. <https://doi.org/10.1002/2017gl072874>
- Yamazaki, D., Trigg, M. A., & Ikeshima, D. (2015). Development of a global ~90 m water body map using multi-temporal Landsat images. *Remote Sensing of Environment*, 171, 337–351. <https://doi.org/10.1016/j.rse.2015.10.014>
- Yoon, T. K., Jin, H., Begum, M. S., Kang, N., & Park, J.-H. (2017). CO<sub>2</sub> outgassing from an urbanized river system fueled by wastewater treatment plant effluents. *Environmental Science & Technology*, 51(18), 10459–10467. <https://doi.org/10.1021/acs.est.7b02344>
- Zhang, S., Lu, X. X., Higgitt, D. L., Chen, C.-T. A., Han, J., & Sun, H. (2008). Recent changes of water discharge and sediment load in the Zhujiang (Pearl River) Basin, China. *Global and Planetary Change*, 60(3–4), 365–380. <https://doi.org/10.1016/j.gloplacha.2007.04.003>
- Zhang, W., Li, H., Xiao, Q., & Li, X. (2021). Urban rivers are hotspots of riverine greenhouse gas (N<sub>2</sub>O, CH<sub>4</sub>, CO<sub>2</sub>) emissions in the mixed-landscape chaohu lake basin. *Water Research*, 189, 116624. <https://doi.org/10.1016/j.watres.2020.116624>

## References From the Supporting Information

- Dickson, A. G., Sabine, C. L., & Christian, J. R. (2007). *Guide to best practices for ocean CO<sub>2</sub> measurements*. North Pacific Marine Science Organization.
- Lehner, B., & Grill, G. (2013). Global river hydrography and network routing: Baseline data and new approaches to study the world's large river systems. *Hydrological Processes*, 27(15), 2171–2186. <https://doi.org/10.1002/hyp.9740>
- Millero, F. J., Graham, T. B., Huang, F., Bustos-Serrano, H., & Pierrot, D. (2006). Dissociation constants of carbonic acid in seawater as a function of salinity and temperature. *Marine Chemistry*, 100(1–2), 80–94. <https://doi.org/10.1016/j.marchem.2005.12.001>
- Ran, L., Li, L., Tian, M., Yang, X., Yu, R., Zhao, J., et al. (2017). Riverine CO<sub>2</sub> emissions in the Wuding River catchment on the Loess Plateau: Environmental controls and dam impoundment impact. *Journal of Geophysical Research: Biogeosciences*, 122(6), 1439–1455. <https://doi.org/10.1002/2016JG003713>
- Tian, M., Yang, X., Ran, L., Su, Y., Li, L., Yu, R., et al. (2019). Impact of land cover types on riverine CO<sub>2</sub> outgassing in the Yellow River source region. *Water*, 11(11), 2243. <https://doi.org/10.3390/w11112243>